DOI: 10.1002/ejic.200901103

Fractal Geometry Approach to Describe Mesostructured Boehmite and Gamma-Alumina Nanorods

Fereshteh Rashidi,*[a,b] Ali Nemati Kharat,*[a] Ali Morad Rashidi,[c] Enrique Lima,[d] Victor Lara,[e] and Jaime S. Valente[f]

Keywords: Boehmite / Alumina / Nanostructures / Fractals / Sol-gel processes / Mesoporous materials / Aluminum

Mesoporous boehmite and gamma-alumina with nanorod-like morphology, exhibiting a high surface area and large pore volume, have been prepared by a nonsurfactant-templating sol–gel technique with a simple precursor system, aluminum isopropoxide, ethanol, 2-propanol, or 2-butanol as solvents, and sulfuric or hydrochloric acid as peptizing agents. The effect of the solvent-type and the peptizing agent were studied, and optimum conditions were determined. A fractal geometry approach was adopted to describe the subtle alterations in the smoothness of the surface as a function of the synthesis conditions. Boehmite and γ-alumina nanorods were characterized by nitrogen physisorption, wide- and small-angle XRD, SAXS, ^{27}Al MAS NMR spectroscopy, TEM, and TGA–DTA. Both boehmite and gamma-alumina nanorods have a large surface area, pore volume, and pore size.

Introduction

Boehmite and alumina constitute an attractive material for industrial applications, mainly because of their low production cost.[1–3] Some of the most common uses of activated alumina are as adsorbents, catalysts, and catalyst supports in several chemical processes. Boehmite (aluminum oxyhydroxide, γ-AlOOH) is the main precursor used to obtain alumina (transition alumina γ-Al_2O_3). On the one hand, extensive demand of various industries for high-purity alumina with a high surface area and large pore volume has made alumina a subject of intensive academic and industrial research,[4–7] as novel approaches for its preparation are required. On the other hand, application of alumina in new processes requires the optimization of some properties, for example, increasing the specific surface area or creating four- and five-coordinate aluminum species (Al^{IV} and Al^{V}, respectively), which are acid centers able to catalyze several chemical reactions. Hence, the control of textural properties (surface area, pore volume, pore size), morphology, and particle size is of the greatest interest to improve the potential of alumina (or even directly boehmite) in catalysis and as composite reinforcements. Apparently, the textural properties of ceramic materials depend on preparatory methods and experimental conditions. In the literature, various boehmite and alumina synthesis procedures under hypercritical drying conditions, with surfactant assemblies, and by using sol–gel or hydrothermal methods, which include aluminum hydroxide precipitated from alkaline solution, aluminum inorganic salts,[8–10] and alkoxide-derived gels,[11] have been investigated in order to control the particle size and morphology, as well as the porosity of the resulting powders. In recent years, sol–gel preparation of ceramic powders has attracted a considerable amount of interest,[1–3,12–14] and the alkoxide-derived alumina gels by the sol–gel method[15] has been shown to be a good technique for controlling the above-mentioned parameters through control of hydrolysis and condensation rates and by variation of temperature, concentration, type of alkoxide, and water-to-alkoxide ratio.[16] Furthermore, aging time,[14,17,18] hypercritical drying conditions,[19,20] surfactant assemblies,[21,22] calcination temperature, and atmosphere could affect the texture of the nanoparticles of boehmite/γ-alumina prepared by the sol–gel technique. Previously, alumina mesostructures containing a transition alumina have been synthesized from aluminum alkoxides or aluminum inorganic salts in the presence of cationic,[23,24] anionic,[25–27] or nonionic triblock copolymer[22,28–30] surfactants as the structure directors. However, the surfactant needs to be removed from the final product, usually by cal-

[a] School of Chemistry, University College of Science, University of Tehran,
P. O. Box 14155-645,Tehran, Iran
Fax: +98-21-66495291
E-mail: rashidi@khayam.ut.ac.ir
alnema@khayam.ut.ac.ir
[b] Department of Complexity Science and Engineering, Graduate School of Frontier Sciences, University of Tokyo, 5-1-5, Kashiwanoha, Kashiwa, Chiba 277-8561, Japan
[c] Nanotechnology Research Center, Research Institute of Petroleum Industry (RIPI), Tehran, Iran
[d] Instituto de Investigaciones en Materiales, Universidad Nacional Autónoma de México, 04510 México D.F., Mexico
[e] Universidad Autónoma Metropolitana, Iztapalapa, Av. San Rafael Atlixco No. 186, Col. Vicentina, 09340 México D.F., Mexico
[f] Instituto Mexicano del Petróleo, Eje Central # 152, 07730 Mexico, D.F., Mexico

cination or extraction; in many cases, the composite was not stable towards the removal of the surfactant.

Nowadays with increasingly stringent environmental legislations, more research for preparing more efficient (texture, acidity, and morphology) supports like alumina for catalytic processes, such as hydrodesulfurization of petroleum cuts, are necessary.[31–33] It has been shown that nanoboehmite, in particular, with defined physical properties is an important material, which can be used in many industries; for instance, the nanoparticles of boehmite can be converted to nanoparticles of γ-Al_2O_3 with potential applications as catalysts and adsorbents. The previous syntheses of similar mesostructured alumina materials have been performed in the presence of surfactants, whereas the present method does not use surfactants. This paper reports a simple sol–gel synthesis procedure for the fabrication of mesostructured nano-boehmite and nano-alumina materials. Synthesis conditions are mild, no surfactant was added to increase the mesoporosity, and chelating agents, commonly used to control the rate of hydrolysis, were not used. The effect of solvent (alcohol) and peptizing agents (inorganic acids) was studied. Variation of these parameters affects the hydrolysis, condensation and polymerization of the aluminum alkoxide, thus modifying many properties of the final material, such as crystallinity, structure, morphology and texture. In this simple manner, boehmite and γ-alumina with excellent textural properties, controllable morphology, high thermal stability and a large amount of Al^V defect centers were obtained. In addition, the fractal dimensions of boehmite and alumina were measured in order to characterize the subtle changes in the surface smoothness.

Results and Discussion

Morphology

Bokhimi et al.[34] reported that during boehmite synthesis, in the initial stage, atoms array to form nanocapsules with shells made up of Al_{13} tridecamers;[35–39] these shells eventually transform into boehmite. At room temperature, this transformation first requires the interaction between the nanocapsules, which opens up the curved structure of their shells and creates conditions for the rearrangement of the distribution of the noncrystalline atoms. Upon slow solvent evaporation, the atoms in the shell regions rearrange from the local order of the Al_{13} tridecamers into the crystalline structure of boehmite, made up of only Al–O octahedra that give rise to thin crystalline boehmite bars, which then order to give boehmite rods. When the boehmite samples were calcined, the morphology produced by their crystallites does not change; the stacking and orientation of the original boehmite layers are preserved. The γ-alumina rods are made of very small γ-alumina crystallites with many interparticle pores created by the loss of the hydroxyl groups of the boehmite during its transformation. Figures 1 and 2 show TEM micrographs of nano-γ-alumina samples, APPSC [alumina prepared with 2-propanol (P) and sulfuric acid (S), calcined (C) after drying] and APBSC [alumina prepared with 2-butanol (B) and sulfuric acid (S), calcined (C) after drying]. These TEM micrographs were taken at different magnifications and are used to exemplify the effect of the solvent on the size and morphology of nano-γ-alumina. Both APPSC and APBSC are made up of nanorods; however, these nanorods are different in size. The APPSC sample (Figure 1) is made up of nanorods whose average dimension and length are 1.80 nm and 43 nm, respectively. For instance, the nanorod denoted A in Figure 1 is 1.13 nm in dimension and 47.5 nm in length.

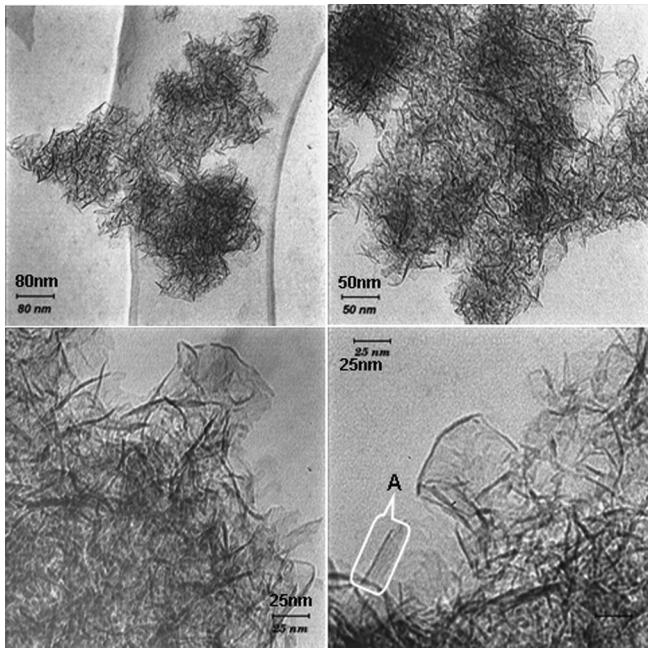

Figure 1. TEM micrographs at different magnifications of the nano-γ-Al_2O_3 prepared with 2-propanol and sulfuric acid (APPSC).

The average dimension and length of the APBSC nanorods sample (Figure 2) are 3.15 nm and 26.1 nm, respectively. For instance, the rod denoted B in Figure 2 is 3.2 nm in dimension and 23.4 nm in length. The TEM study of all samples indicates that with decreasing number of carbon atoms in the alcohol, the particles are bigger.

Shen et al.[40a] reported that boehmite and alumina nanorods can be prepared by a nontemplate route with lengths and diameters in the range 100–400 and 20–30 nm, respectively. Further, Zhu et al.[40c] reported that AlOOH nanofibers can be assembled in the presence of non-ionic poly(ethylene glycol) (PEO) surfactant; the maximum length of the fibers was found to be 100 nm. Relative to previous reports,[40a,40c] these γ-alumina nanorods are smaller in dimension and length, which could have a significant effect on the textural properties, as seen by the higher surface area determined by N_2 physisorption (vide infra). The nanorod morphology can be determined by measuring the fractal dimension by using SAXS or SANS under dilute conditions; it is important to note that this has not been done

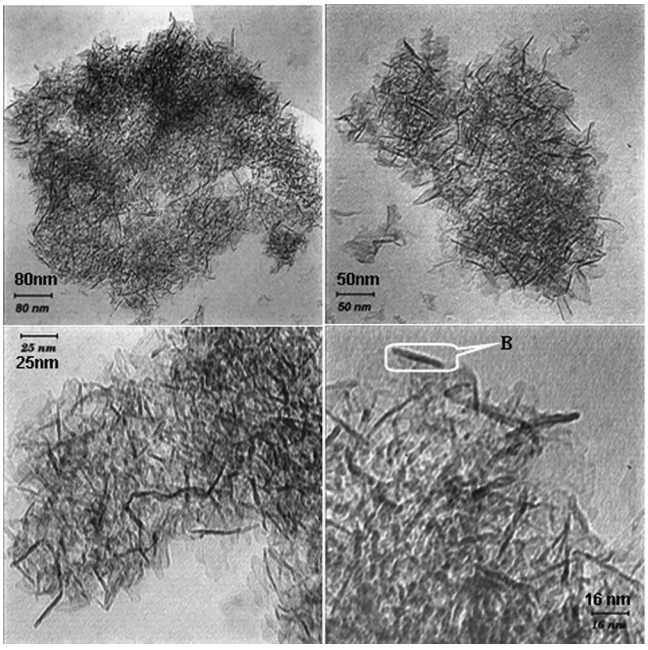

Figure 2. TEM micrographs at different magnifications of the nano-γ-Al_2O_3 prepared with 2-butanol and sulfuric acid (APBSC).

for the other reported alumina nanorods.[34,40a,40b,40c] The Kratky plots for both the boehmite and alumina samples (Figure 3) have a region at moderate angles where the intensity is related to h^{-2} (h is the angular parameter, defined as $h = 2\pi \sin\theta/\lambda$, where θ and λ are the X-ray scattering angle and the wavelength, respectively), and at higher angles, the scattering intensity tends to be proportional to h^{-1}. The scattering profiles show a monotonically increasing curve. These profiles are typical for objects that are inclined to be purely one-dimensional and extend linearly, such as rods or fibrous particles.[41–43] The SAXS results are in total agreement with the electronic microscopy results. The SAXS profiles shown in Figure 3 are very useful, because they confirm the shape of the scattered objects.

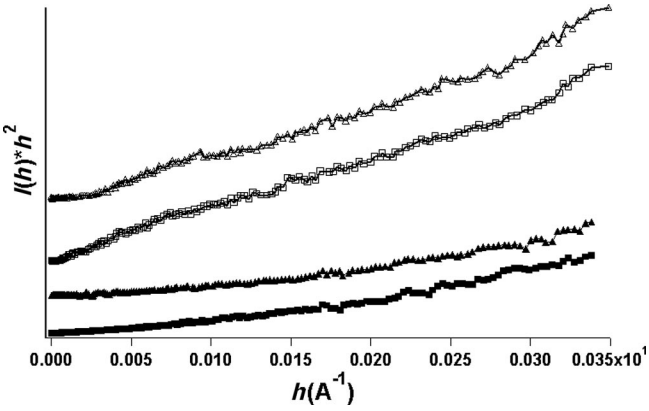

Figure 3. SAXS Kratky profiles of nano-boehmite (filled symbols) and nano-γ-Al_2O_3 samples (open symbols): (-■-) APES, (-▲-) APBS, (-□-) APESC and (-Δ-) APBSC.

Textural Properties

The specific surface area, pore diameter, and pore volume of the prepared nano-boehmite and nano-γ-Al_2O_3 samples are reported in Table 1. From Table 1, it can be noticed that with increasing number of carbon atoms of the solvent, the pore volume and pore diameter of both the boehmite and alumina samples increase; by considering the experimental error of the BET model (ca. 10%), all samples have almost the same surface areas, with the exception of the sample APES [boehmite prepared with ethanol (E) and sulfuric acid (S)]. The exceptionally large surface area of APES (469 $m^2 g^{-1}$) results from the large pore volume and small average pore size. According to IUPAC classification, all the N_2 physisorption isotherms of the boehmite and calcined samples are of type IV, as can be seen in Figures 4a and 5a, which characterizes them as mesoporous solids. When the samples were calcined, no important changes were observed in the hysteresis loops. The hysteresis loop for the APECl [boehmite prepared with ethanol (E) and hydrochloric acid (Cl)] and APEClC [alumina prepared with ethanol (E) and hydrochloric acid (Cl), calcined (C) after drying] samples are of the H2 type,[44] which is in agreement with randomly folded boehmite sheets of solids.[45] But in the other samples {APES, APPS [boehmite prepared with 2-propanol (P) and sulfuric acid (S)], APBS [boehmite prepared with 2-butanol (B) and sulfuric acid (S)], APESC [alumina prepared with ethanol (E) and sulfuric acid (S), calcined (C) after drying], APPSC, and APBSC}, the hysteresis loops are of type H1, which is in agreement with uniformly folded boehmite sheets of solids, a homogeneous pore-size distribution, and a uniform particle size. Pore size plots of boehmite and alumina samples (Figures 4b and 5b) show that they are narrowly distributed. It can be noticed that the pore volume and pore size of all the samples increase when H_2SO_4 is used instead of HCl and also when the alcohol with the highest number of carbon atoms is used. The highest pore volume values are reached with the samples APBS and APBSC (1.62 and 1.65 $cm^3 g^{-1}$, respectively). This behavior is in agreement with the hysteresis evolution observed as a function of type of acid and alcohol. Hence, as it was shown in previous work,[17] the ordering of boehmite sheets during aging takes place, which points to an unfinished stacking process of the boehmite phase. The importance of high pore volume in catalysts/catalyst supports is reflected in the total volume of the final reactor or vessel, which will be smaller, and thus economic, in terms of catalyst and/or support masses.

It was observed that the textural parameters, which are very important in catalysis, could be regulated easily by choosing adequate conditions of synthesis and post-treatment of the solids. Actually, the catalytic process involves dynamic interfacial phenomena, which in turn are determined by surface irregularities. In this finding, fractal dimension values from Table 1 are more relevant as they represent a measure of the smoothness or irregularity of the surface. Although rods must have a fractal dimension close to 1, the values included in Table 1 range between 2 and 3

Table 1. Textural properties of nano-boehmite and nano-γ-Al_2O_3 samples.

Sample	BET surface area ($m^2 g^{-1}$)	Total pore volume ($cm^3 g^{-1}$)	Av. pore size (Å)	Fractal dimension[a]
APEClI	373	0.74	70.5	2.43
APES	469	1.07	70.5	2.45
APPS	380	1.18	90.5	2.42
APBS	398	1.62	109.6	2.51
APEClC	411	0.41	37.1	2.75
APESC	410	1.16	70.5	2.69
APPSC	404	1.27	71.4	2.50
APBSC	432	1.65	90.0	2.48

[a] As determined from SAXS data and following the Porod Law.

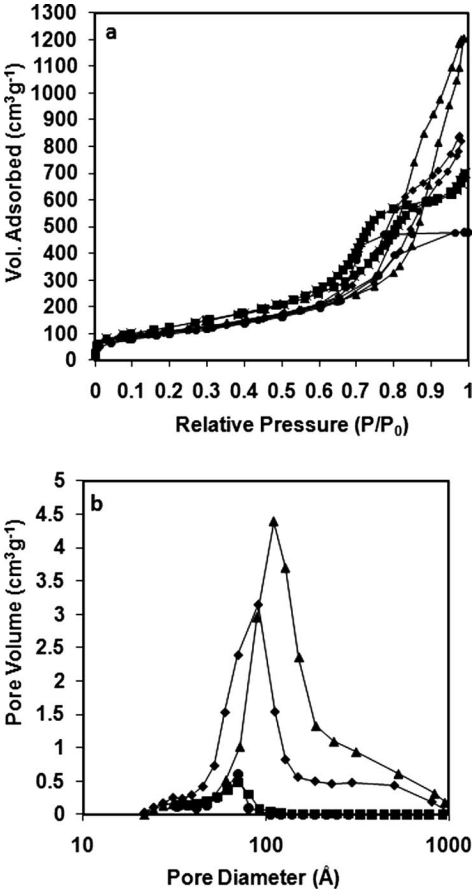

Figure 4. (a) Adsorption–desorption isotherms and (b) pore-size distributions of nano-boehmite samples: (-●-)APEClI, (-■-) APES, (-♦-) APPS and, (-▲-)APBS.

because the alumina and boehmite rods are not rigid but porous,[41,43,46,47] we have then non-solid rods but fractal objects with different surface/volume ratio. One can see that the fractal dimension values of both boehmite and alumina samples are similar. It seems, however, that the alumina samples prepared in the presence of ethanol are materials with more surface defects. This result can be explained because of the presence of the five-coordinated aluminum at the surface of these samples, as shown by ^{27}Al NMR spectroscopy. Furthermore, note that samples exhibiting the highest surface area (APES and APBSC) are not necessarily

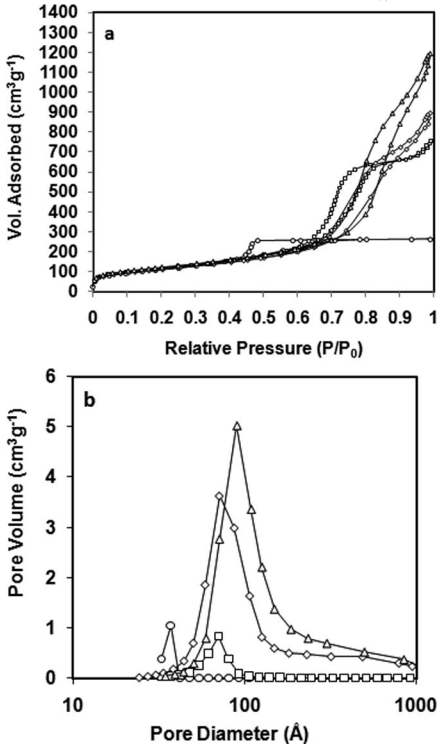

Figure 5. (a) Adsorption–desorption isotherms and (b) pore-size distributions of nano-γ-Al_2O_3 samples: (-○-)APEClC, (-□-) APESC, (-◇-)APPSC, and (-Δ-)APBSC.

those with the highest fractal dimension. It is worth mentioning that SAXS measurements are sensitive to differences in the electron density, and the BET surface is measured only from the open pores, and bubbles, for example, are not taken into account.

The previous synthesis of similar mesostructured alumina materials have been performed in the presence of surfactants; Pinnavaia et al. reported the preparation of mesostructured alumina materials (designated as MSU-X alumina), with substantially improved surface area and porosity, from aluminum *sec*-butoxide in the presence of electrically neutral block copolymer surfactants as the structure director.[31] They also prepared another kind of mesostructured alumina material (designated as MSU-gamma alumina) with exceptional surface area (300–350 $m^2 g^{-1}$) and pore volume (0.45–0.75 $cm^3 g^{-1}$), from $Al(NO_3)_3$ or $AlCl_3$ in the presence of nonionic triblock copolymer surfactants as the structure director.[26] M. Akia et al. reported the preparation of mesostructured gamma alumina materials, from aluminum isopropoxide and a cationic surfactant; they obtained a maximum surface area of 396.5 $m^2 g^{-1}$, pore size of 13.26 nm, and a pore volume of 1.71 $cm^3 g^{-1}$.[32] Although there are some reports on a nonsurfactant-templating route for the preparation of alumina nanorods, no information is available on their textural properties[40a] and the obtained surface area is low (50–250 $m^2 g^{-1}$).[40b] Our present method also does not use surfactants; however, the obtained surface area (373–469 $m^2 g^{-1}$) and pore volume (0.74–1.62 $cm^3 g^{-1}$) are higher.

Structural Properties

All the sol–gel boehmite samples (Figure 6) have a diffraction pattern similar to that of crystalline boehmite (JCPDS 21-1307); the only exception is that the (0 2 0) reflection is missing. This indicates a poor ordering of the stacked layers of boehmite. This might be due to the presence of OR groups from the alkoxide precursor, as the amount of remaining OR groups in the dry solids is controlled by the alkoxide/water ratio. A high ratio gives a partially alkoxylated boehmite phase. Said alkoxy groups may be intercalated between the boehmite layers, distorting the unit cell. Furthermore, the (1 2 0) diffraction peak appears shifted to a lower angle, relative to that of crystalline boehmite (Figure 6), indicating that the distance between (1 2 0) planes is larger in these samples. This distance is related to hydrogen bonding between layers;[49] therefore, hydrogen bonds are weaker. The type of solvent and acid had a marked effect on this parameter; when the number of carbon atoms in the alcohol is increased and sulfuric acid is employed, a more symmetric and sharper (1 2 0) peak is produced (see Figure 6). The high-angle XRD patterns obtained after calcination of the boehmite at 550 °C (γ-Al_2O_3) are shown in Figure 7; the diffraction peaks of all the samples can be indexed to the γ-Al_2O_3 phase (JCPDS 29-63), and the diffraction patterns for all samples are essentially equal.

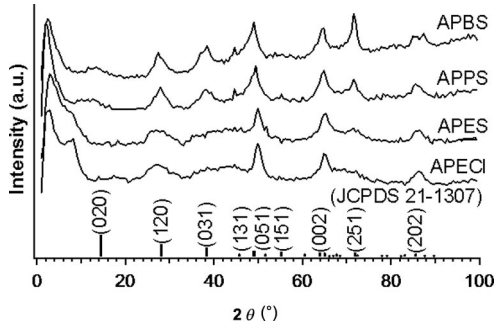

Figure 6. Wide-angle powder X-ray diffraction patterns of the nano-boehmite samples.

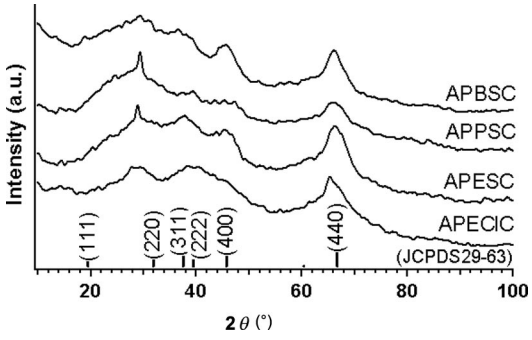

Figure 7. Wide-angle powder X-ray diffraction patterns of the nano-γ-Al_2O_3 samples.

Well-resolved diffraction peaks at low angles support that large spacing between crystalline planes are well defined, i.e. a mesostructure is present. Valente et al.[17] reported on boehmite samples in which the atoms are ordered at long distances, which gives rise to two diffraction peaks at 2θ angles lower than 10°. However, in this study (Figures 8 and 9), with exception of the sample prepared with HCl (APEClI), only one peak is observed, and its 2θ value is greater (2–3°). The increasing intensity of the low-angle peak as the solvent chain increases (higher number of carbon atoms of the solvent) indicates that the mesostructure is more clearly defined. It is possible that the solvent alcohol is acting as a structure-directing agent.[50] It was also observed that APEClI and APES do not have the same crystalline structure, because their diffraction pattern differs at low angles. The low diffraction angles of the γ-alumina samples (Figure 9) were measured in detail. The patterns for all the samples have a peak with its maximum between 2 and 3°; the peak of the APPSC sample has the highest intensity.

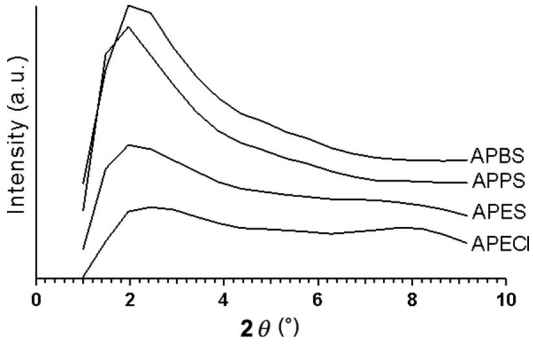

Figure 8. Low-angle powder X-ray diffraction patterns of the nano-boehmite samples.

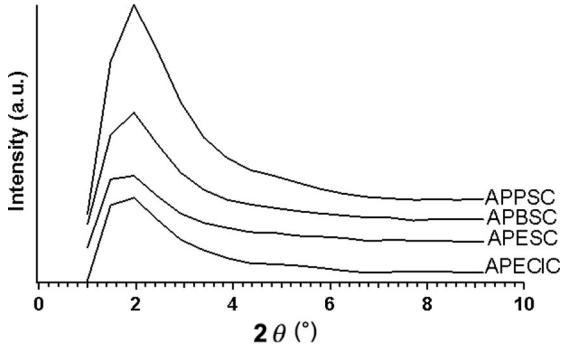

Figure 9. Low-angle powder X-ray diffraction patterns of the nano-γ-Al_2O_3 samples.

The crystal size of the samples can be estimated from the peak broadening in the XRD patterns. For instance, in Figure 7, the peak broadening of the calcined samples follows the order: APEClC ≈ APESC > APBSC > APPSC. The average crystallite size, as calculated from the half-width of the diffraction peaks by using the Scherrer equation, are in the order: APEClC = APESC (≈23.4 nm) < APBSC (35.9 nm) < APPSC (56.5 nm); these results are similar to the size of the nanorods, as shown by the TEM images (Figures 1 and 2).

Figure 10 displays the ^{27}Al MAS NMR spectra of fresh samples, and shows that the aluminum remains predominantly six-coordinate in an oxygen environment (signal close to 3 ppm), irrespective of the alcohol used during the sol–gel synthesis. With regard to the position and intensity of the ^{27}Al NMR signals, no significant differences are observed for the set of spectra. Thus, it should be assumed that water molecules contained in the boehmite samples are enough to homogenize the environment of the aluminum unsaturated centers, if any, produced during synthesis. Figure 11 includes the ^{27}Al MAS NMR spectra of the γ-Al_2O_3 samples (calcined samples). In all four samples, two signals are observed. The first signal, at about 3 ppm, is assigned to six-coordinate aluminum (Al^{VI}), and the second signal, at δ = 65 ppm, is assigned to four-coordinate aluminum (Al^{IV}). In addition, in the samples APEClC and APESC, a third isotropic peak is evident at δ = 32 ppm, which can be assigned to five-coordinate aluminum (Al^{V}). In the sample APBSC, no resonance for Al^{V} is observed, and in the sample APPSC, this peak is almost negligible. Many reports suggest that Al^{V} is formed as a consequence of the creation of structure defects. Thus, among the alcohols used, only butanol does not induce the formation of Al^{V}, which suggests that longer alkyl chains in the solvent alcohol stimulates the formation of longer polymeric chains during aging of gel. This feature could be favorable for developing higher specific surface areas, but the formation of acid centers is inhibited. Ethanol is therefore better for inducing the formation of acid unsaturated sites.

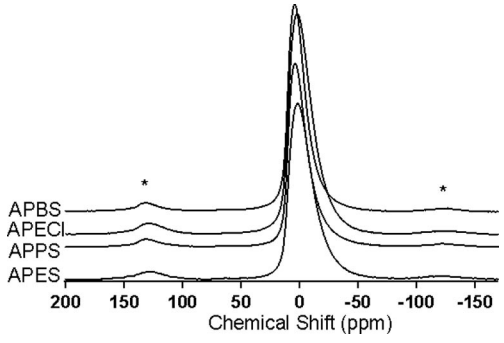

Figure 10. ^{27}Al MAS NMR spectra of the nano-boehmite samples. The asterisks indicate spinning side bands (spinning rate 10 kHz).

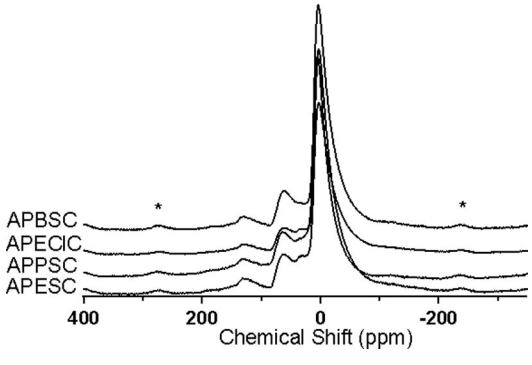

Figure 11. ^{27}Al MAS NMR spectra of the nano-γ-Al_2O_3 samples. The asterisks indicate spinning side bands (spinning rate 10 kHz).

Thermal Properties

The differential thermal analysis (DTA) and the thermogravimetric analysis (TGA) curves of the boehmite nanorods prepared with HCl and ethanol (APECl), with H_2SO_4 and 2-propanol (APPS), and with H_2SO_4 and 2-butanol (APBS) are shown in Figure 12.

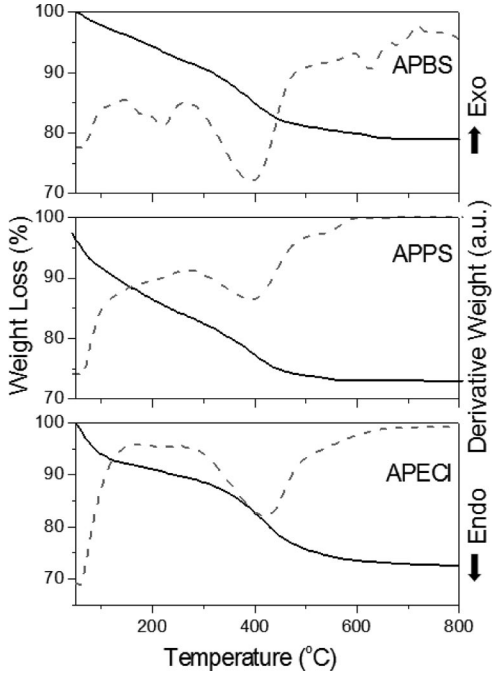

Figure 12. Thermogravimetric and differential thermal analysis of the nano-boehmite samples.

DTA of pure boehmite materials show a wide endothermic peak below 200 °C, which arises from the removal of hydration water and an endothermic peak at higher temperatures related to the phase transition to γ-Al_2O_3.[48,51] In general, APECl shows three main thermal events: (i) a small endothermic peak at 150 °C, which probably can be assigned to evaporation and/or desorption of encapsulated water from condensation, solvent, and organic compounds from the gelation reaction, (ii) a small exothermic peak at 240 °C, which can be attributed to the combustion and decomposition of the organic compounds (residual alkoxy groups), and (iii) an endothermic peak at 425 °C, which arises from the dehydroxylation of boehmite crystallites and transformation into γ-alumina. In contrast, DTA patterns of APPS and APBS differ from that of APECl in that: (i) the exothermic peak shifts to 260 °C and (ii) the second endothermic peak not only shifts to 400 °C, but its broad shape indicates a nonuniform dehydroxylation process. This behavior can be rationalized in terms of two effects: (i) the population of hydroxyl groups on the surface of the crystallites and (ii) the location of sulfate groups,[52] that is, alumina samples prepared with HCl have a greater number of hydroxyl groups than sulfated alumina samples. The DTA results therefore show that the transformation temperature of boehmite into γ-alumina depends on the solvents and inorganic acids.

The TGA curves of APECl, APPS, and APBS show a total weight loss of 28.19, 27.02, and 21.72%, respectively. The curves show three stages of weight loss at different temperatures: (i) up to 180 °C, which is attributable to the loss of adsorbed water, (ii) between 180 and 260 °C, which corresponds to the combustion of residual alkoxy groups, as is evident from the corresponding DTA curve, and (iii) between 260 and 500 °C, which corresponds to the loss of structural water (decomposition of structural –OH groups) and to the transformation of boehmite into γ-alumina.

Conclusions

We have prepared mesoporous boehmite and γ-alumina with nanorod-type morphology, with an average dimension of 2.5 nm and length of 50 nm, through a nontoxic and nonsurfactant-templating route. The sol–gel method was used with aluminum triisopropoxide as the aluminum precursor and ethanol, 2-propanol, or 2-butanol as the solvent. The obtained materials (boehmite and γ-alumina nanorods) display high surface areas (as high as 469 $m^2 g^{-1}$), a high total pore volume (as high as 1.65 $cm^3 g^{-1}$), uniform pore sizes (up to 109.6 Å), and a one dimensional interconnected rodlike mesostructures. The textural parameters of the samples can be tuned by adjusting the synthesis conditions. The fractal dimension parameter is also highly affected by the synthesis conditions. If the synthesis is carried out in the presence of ethanol, aluminum unsaturated sites are formed at the surface and the fractal dimension value increases. Additionally, mesoporous γ-alumina nanorods with both a high surface area (411–432 $m^2 g^{-1}$) and a high total pore volume (0.4–1.65 $cm^3 g^{-1}$) can be obtained even after calcination at 550 °C. Concomitantly, different inorganic acids and solvents can be used to adjust the average pore size from 37.1 to 109.6 Å. Moreover, the tunable pore sizes and the high total pore volume suggest that these mesoporous alumina materials could be ideal supports for heterogeneous catalysis, for example, in the hydrotreating reaction.

Experimental Section

Synthesis: Aluminum triisopropoxide (ATP) (Fluka, 99%) was used as the aluminum source. Sulfuric acid (Across, 96%) or hydrochloric acid (Merck, 37%) were used as the hydrolysis catalyst. Ethanol (Merck, 99%), 2-propanol (Merck, 99%), or 2-butanol (Merck, 99%) were used as the solvents. The synthesis procedure was as follows: aluminum triisopropoxide (ATP) was dissolved in the desired alcohol (ethanol, 2-propanol, or 2-butanol), and the mixture was heated at reflux and stirred for 1 h. Hydrochloric acid or sulfuric acid was then added dropwise, while the mixture was stirred and refluxed for a further 3 h. The system was cooled down to room temperature; at this point water was added, which allowed for completion of hydrolysis. A transparent gel was obtained when hydrochloric acid was used, while when sulfuric acid was used the gel was slightly turbid. The molar ratios of the reactants were: ATP/ROH = 1:60, ATP/acid = 1:0.04, and H_2O/ATP = 1:1. The gel was poured in a glass vessel and left to age for 30 d. Thereafter, the product was dried overnight at 100 °C. The dried samples (boehmite) were labeled as APECl, APES, APPS, and APBS, according to the alcohol (E, P, and B correspond to EtOH, 2-PrOH, and 2-BuOH, respectively) and acid type (Cl and S correspond to HCl and H_2SO_4, respectively). The dried solids were calcined in air from room temperature up to 550 °C; they remained at this temperature for 6 h. These calcined solids (γ-Al_2O_3) were identified by adding the letter (C) to the nomenclature used for the fresh sample, i.e. APEClC, APESC, APPSC, and APBSC.

Characterization

Morphology: The samples were analyzed by transmission electron microscopy, in a 120 kVLEO-912AB (ZIES). The samples were dispersed in ethanol before they were placed in the copper grid with holey carbon film support. A Kratky camera coupled to a copper anode tube was used to measure the small-angle X-ray scattering (SAXS) curves. The distance between the sample and the linear proportional counter was 25 cm; a Ni filter selected the Cu-K_α radiation. The sample was introduced into a capillary tube. The intensity $I(h)$ was measured for 9 min in order to obtain good quality statistics. The SAXS data were processed with the ITP program,[53–56] where the angular parameter, h, is defined as $h = 2\pi\sin\theta/\lambda$, where θ and λ are the X-ray scattering angle and the wavelength, respectively. The shape of the scattering objects was estimated from the Kratky plot, i.e. $h^2I(h)$ against h. The shape is determined by the shape of the Kratky curve: for instance, if the curve presents a peak, the particles are globular.[57] Furthermore, under the Porod Law, from the slope of the curve $\log I(h)$ vs. $\log(h)$, the fractal dimension of the scattering objects can be determined.[58,59]

Texture: The specific surface area, pore volume, and porosity distribution of the boehmite and calcined samples were obtained from nitrogen adsorption–desorption isotherms, determined at –196 °C with an ASAP 2010 apparatus. Surface areas were calculated by the Brunauer–Emmett–Teller (BET) method, and the pore-size distribution and total pore volume were determined by the Brunauer–Joyner–Hallenda (BJH) method. Prior to adsorption, the samples were outgassed at 125 °C (boehmite) or at 300 °C (γ-Al_2O_3) for 4 h under a residual pressure of 10^{-4} Torr.

Structure: X-ray diffraction patterns of the samples packed in an aluminum glass holder were recorded at room temperature with Cu-K_α radiation with a Philips PW-1840 diffractometer with a theta–theta configuration. The diffraction intensity was measured in the 2θ range between 1 and 100°, with a 2θ step of 0.01° and 0.2 s per point. Low-angle measurements were performed from 1 to 10°, with a 2θ step of 0.01 and 2 s per point. One-pulse solid-state ^{27}Al MAS NMR spectra were acquired at a frequency of 78.15 MHz on a Bruker Avance II spectrometer by using a 4-mm MAS probe with a spinning rate of 10 kHz. Short single pulses ($\pi/12$) were used with a recycle time of 0.5 s. The ^{27}Al chemical shifts were referenced by using a 1 N aqueous solution of Al $(NO_3)_3$ as the external reference.

Thermal Analysis: The weight loss and phase transformation associated to temperature were determined by thermogravimetry and differential thermal analysis with a Mettler Swiss SDTA 851 apparatus. Samples were heated in an air flow of 60 $cm^3 min^{-1}$ from room temperature to 1000 °C at a heating rate of 5 °C min^{-1}.

[1] L. Ji, J. Lin, K. L. Tan, H. C. Zeng, *Chem. Mater.* **2000**, *12*, 931–939.
[2] B. E. Yoldas, *J. Appl. Chem. Biotechnol.* **1973**, *23*, 803–809.
[3] B. E. Yoldas, *Am. Ceram. Soc. Bull.* **1975**, *54*, 286–288.
[4] J. Sánchez-Valente, F. Hernández-Beltrán, M. L. Guzmán-Castillo, J. J. Fripiat, X. Bokhimi, *J. Mater. Res.* **2004**, *19*, 1499–1503.

[5] T. Kotanigawa, M. Yamamoto, M. Utiyama, H. Hattori, K. Tanabe, *Appl. Catal.* **1981**, *1*,185–200.
[6] B. Beguin, E. Garboswki, M. Primet, *J. Catal.* **1991**, *127*, 595–604.
[7] H. Knözinger, P. Ratnasamy, *Catal. Rev. Sci. Eng.* **1978**, *17*, 31–70.
[8] G. K. Chuan, S. Jaenicke, T. H. Xu, *Microporous Mesoporous Mater.* **2000**, *37*, 345–353.
[9] D. Mishra, S. Anand, R. K. Panda, R. P. Das, *Mater. Lett.* **2000**, *42*, 38–45.
[10] D. Mishra, S. Anand, R. K. Panda, R. P. Das, *Mater. Lett.* **2002**, *53*, 133–137.
[11] B. E. Yoldas, *J. Mater. Sci.* **1975**, *10*, 1856–1860.
[12] R. Nass, H. Schmidet, *J. Non-Cryst. Solids* **1990**, *121*, 329–333.
[13] F. Vaudry, S. Khodabandeh, M. E. Davis, *Chem. Mater.* **1996**, *8*, 1451–1464.
[14] J. Ray, M. Chatterjee, D. J. Ganguli, *J. Mater. Sci. Lett.* **1993**, *12*, 1755–1757.
[15] M. A. Cauqui, J. M. Rodriguez-Izquierdo, *J. Non-Cryst. Solids* **1992**, *148*, 724–738.
[16] J. A. Schwarz, C. Contescu, A. Contescu, *Chem. Rev.* **1995**, *95*, 477–510.
[17] J. S. Valente, X. Bokhimi, J. A. Toledo, *Appl. Catal. A* **2004**, *264*, 175–179.
[18] J. Livage, *Catal. Today* **1998**, *41*, 3–19.
[19] G. M. Pajonk, *Catal. Today* **1997**, *35*, 319–337.
[20] M. Schneider, A. Baiker, *Catal. Rev. Sci. Eng.* **1995**, *37*, 515–556.
[21] M. Yada, H. Hiyoshi, K. Ohe, M. Machida, T. Kijima, *Inorg. Chem.* **1997**, *36*, 5565–5569.
[22] Z. Zhang, T. J. Pinnavaia, *J. Am. Chem. Soc.* **2002**, *124*, 12294–12301.
[23] S. Cabrera, J. El Haskouri, J. Alamo, A. Beltran, D. Beltran, S. Mendioroz, M. D. Marcos, P. Amoros, *Adv. Mater.* **1999**, *11*, 379–381.
[24] M. Akia, S. M. Alavi, M. Rezaei, Z. F. Yan, *Microporous Mesoporous Mater.* **2009**, *122*, 72–78.
[25] M. Yada, M. Machida, T. Kijima, *Chem. Commun.* **1996**, 769–770.
[26] M. Yada, M. Ohya, M. Machida, T. Kijima, *Chem. Commun.* **1998**, 1941–1942.
[27] V. Gonzalez-Pena, I. Diaz, C. Marquez-Alvarez, E. Sastre, J. Perez-Pariente, *Microporous Mesoporous Mater.* **2001**, *44–45*, 203–210.
[28] P. Yang, D. Zhao, D. I. Margolese, B. F. Chmelka, G. D. Stucky, *Chem. Mater.* **1999**, *11*, 2813–2826.
[29] P. D. Yang, D. Y. Zhao, D. I. Margolese, B. F. Chmelka, G. D. Stucky, *Nature* **1998**, *396*, 152–155.
[30] A. S. Bagshaw, T. J. Pinnavaia, *Angew. Chem. Int. Ed. Engl.* **1996**, *35*, 1102–1105.
[31] Q. Liu, A. Wang, X. Wang, T. Zhang, *Microporous Mesoporous Mater.* **2006**, *92*, 10–21.
[32] C. Misra, *Industrial Alumina Chemicals*, ACS Monograph, American Chemical Society, Washington, DC, **1986**, vol. 184.
[33] Cejka, *J. Appl. Catal. A* **2003**, *254*, 327–338.
[34] X. Bokhimi, X. E. Lima, J. S. Valente, *J. Phys. Chem. B* **2005**, *109*, 22222–22227.
[35] W. V. Rausch, H. D. Bale, *J. Chem. Phys.* **1964**, *40*, 3391–3394.
[36] G. Johansson, *Acta Chem. Scand.* **1960**, *14*, 771–773.
[37] L. Allouche, C. Gearardin, T. Loiseau, G. Fearey, F. Taulelle, *Angew. Chem. Int. Ed.* **2000**, *39*, 511–514.
[38] M. Nyman, F. Bonhomme, T. M. Alam, M. A. Rodriguez, B. R. Cherry, J. L. Krumhansl, T. M. Nenoff, A. M. Sattler, *Science* **2002**, *297*, 996–998.
[39] M. Sugeta, T. Yamase, *Acta Crystallogr., Sect. C* **1997**, *53*, 1166–1170.
[40] a) S. C. Shen, Q. Chen, P. S. Chow, G. H. Tan, X. T. Zeng, Z. Wang, B. H. Tan Reginald, *J. Phys. Chem. C* **2007**, *111*, 700–707; b) J. P. Sterte, J.-E. Otterstedt, *Mater. Res. Bull.* **1986**, *21*, 1159–1166; c) H. Y. Zhu, J. D. Riches, J. C. Barry, *Chem. Mater.* **2002**, *14*,2086–2093.
[41] G. Beaucage, *J. Appl. Crystallogr.* **1996**, *29*, 134–146.
[42] J. M. Flanagan, M. Kataoka, M. Fugisawa, D. M. Engelman, *Biochemistry* **1993**, *32*, 10359–10379.
[43] A. Guzmán-Vargas, E. Lima, G. Delahay, B. Coq, V. Lara, *Ind. Eng. Chem. Res.* **2006**, *45*, 4163–4168.
[44] K. S. W. Singh, D. H. Everett, R. A. W. Haul, L. Moscou, R. A. Pierotti, J. Rouquerol, T. Siemieniewska, *Pure Appl. Chem.* **1985**, *57*, 603–619.
[45] J. Sánchez-Valente, X. Bokhimi, F. Hernández, *Langmuir* **2003**, *19*, 3583–3588.
[46] D. Avnir, D. Farin, P. Pfeifer, *Nature* **1984**, *308*, 261–263.
[47] B. Yu, J. Li, *Fractals* **2004**, *12*, 17.
[48] X. Bokhimi, J. A. Toledo, M. L. Guzmán, M. Mar, F. Hernández, J. Navarrete, *J. Solid State Chem.* **2001**, *161*, 319–326.
[49] X. Bokhimi, X. J. S. Valente, F. Pedraza, *J. Solid State Chem.* **2002**, *166*, 182–190.
[50] J. S. Valente, J. Prince, A. M. Maubert, L. Lartundo-Rojas, P. Del Angel, G. Ferrat, J. G. Hernandez, E. Lopez-Salinas, *J. Phys. Chem. C* **2009**, *113*, 5547–5555.
[51] M. L. Guzmán-Castillo, X. Bokhimi, J. A. Toledo, J. Salmones-Blásquez, F. Hernández-Beltrán, *J. Phys. Chem. A* **2001**, *105*, 2099–2105.
[52] J. S. Valente, S. Falcon, E. Lima, M. A. Vera, P. Bosch, E. Lopez-Salinas, *Microporous Mesoporous Mater.* **2006**, *94*, 277–282.
[53] O. Glatter, *J. Appl. Crystallogr.* **1981**, *14*, 101–108.
[54] O. Glatter, B. Hainisch, *J. Appl. Crystallogr.* **1984**, *17*, 435–441.
[55] O. Glatter, *J. Appl. Crystallogr.* **1988**, *21*, 886–890.
[56] O. Glatter, *Prog. Colloid Polym. Sci.* **1991**, *84*, 46–54.
[57] O. Glatter, K. Gruber, *J. Appl. Crystallogr.* **1993**, *26*, 512–518.
[58] M. Kataoka, J. M. Flanagan, F. Tokunaga, D. M. Engelman in *Synchrotron Radiation in the Biosciences* (Eds.: B. Chanse, J. Deisenhofer, S. Ebashi, D. T. Goodhead, H. E. Huxley), Clarendon Press, Oxford, U. K., **1994**; vol. 4, p. 87.
[59] J. E. Martin, A. J. Hurd, *J. Appl. Crystallogr.* **1987**, *20*, 61–78.

Received: November 14, 2009
Published Online: February 23, 2010

